Chameleon Halo Modeling in $f(R)$ Gravity

Yin Li[1,2] and Wayne Hu[1,3]

[1] *Kavli Institute for Cosmological Physics, University of Chicago, Chicago IL 60637*
[2] *Department of Physics, University of Chicago, Chicago IL 60637*
[3] *Department of Astronomy & Astrophysics, University of Chicago, Chicago IL 60637*

(Dated: July 27, 2011)

We model the chameleon effect on cosmological statistics for the modified gravity $f(R)$ model of cosmic acceleration. The chameleon effect, required to make the model compatible with local tests of gravity, reduces force enhancement as a function of the depth of the gravitational potential wells of collapsed structure and so is readily incorporated into a halo model by including parameters for the chameleon mass threshold and rapidity of transition. We show that the abundance of halos around the chameleon mass threshold are enhanced by both the merging from below and the lack of merging to larger masses. This property also controls the power spectrum in the nonlinear regime and we provide a description of the transition to the linear regime that is valid for a wide range of $f(R)$ models.

I. INTRODUCTION

The modified action $f(R)$ model for cosmic acceleration provides a concrete framework under which to relate local and cosmological tests of gravity. Here the Einstein-Hilbert action is augmented with a general function of the Ricci scalar curvature in such a way as to mimic the cosmological constant at cosmologically low curvature [1–3].

The extra scalar degree of freedom df/dR mediates an enhanced gravitational force on scales smaller than its Compton wavelength. In order to hide this enhancement from local tests of gravity, viable models employ the chameleon mechanism [4, 5] where the Compton wavelength can shrink in regions of deep gravitational potential wells. If one assumes that the $f(R)$ model is a complete description of gravity from solar system scales to cosmology, local tests in conjunction with minimal assumptions about the Galactic potential place a stringent bound on $f(R)$ models. Namely the cosmological amplitude of the field $|f_{R0}|$ must be less than a few times 10^{-6} [6].

Currently the tightest cosmological bounds come from the lack of an excess in the abundance of the most massive dark matter halos or galaxy clusters [7, 8]. The bound on the field amplitude depends on the model but generally lie above the 10^{-5} level for models that seek to diminish the modification at high redshift [9]. Thus cosmological constraints currently are at best approaching the level of solar system tests. On the other hand they test these modifications on a vastly different scale and it is possible that $f(R)$ is just an effective theory only strictly valid on cosmological scales.

As cosmological data continue to improve, they will soon begin to probe a regime where cosmology is directly competitive with solar system tests in the full $f(R)$ context. Here the chameleon mechanism becomes important for all halos of mass comparable to or greater than the Galaxy. This regime is substantially more difficult to characterize due to the non-linearity in the field equation for the enhanced force.

Under the halo model approach, the first step in understanding cosmological statistics associated with the observable properties of dark matter halos is to characterize the mass function. Previous attempts to model the mass function of simulations have not been able to capture the abundance of intermediate mass halos once the chameleon mechanism becomes active. This abundance is doubly enhanced since the extra force augments merging of low mass halos into intermediate mass halos whereas the chameleon effect shuts down merging of intermediate mass halos to high mass halos.

Based on a mass function model, we can build a parameterized post-Friedmann (PPF) description of the chameleon effect in cosmological statistics such as the dark matter power spectrum. Whereas previous PPF approaches have been based on density thresholds [10] and are appropriate for models that utilize the Vainshtein mechanism, they require extensive ad hoc modifications for the chameleon mechanism [11]. The problem is that the chameleon mechanism should be parameterized in terms of a proxy for the depth of gravitational potential wells, which in the halo model can be readily associated with the mass of dark matter halos.

The outline of the paper is as follows. In §II, we briefly review the $f(R)$ model and simulations. We parameterize the chameleon effect in the mass function in §III, which we use in §IV to characterize the nonlinear dark matter power spectrum. We discuss these results in §V.

II. $f(R)$ SIMULATIONS

In $f(R)$ models, the Einstein-Hilbert action is augmented with a general function of the scalar curvature R

$$S_G = \int d^4x\sqrt{-g}\left[\frac{R+f(R)}{16\pi G}\right]. \quad (1)$$

Here and throughout $c = \hbar = 1$. For definiteness we take the high curvature limit of the models in [6]

$$f(R) \approx -2\Lambda - \frac{f_{R0}}{n}\frac{\bar{R}_0^{n+1}}{R^n}\,, \tag{2}$$

where the constant $\bar{R}_0$ is the background scalar curvature R today in a ΛCDM cosmology with a cosmological constant Λ. Here f_{R0} is a parameter that controls the amplitude of the field $f_R \equiv df/dR$ at the background curvature today. Note that viable models have $|f_{R0}| \ll 1$ and expansion histories that are observationally indistinguishable from ΛCDM.

Gravitational force enhancements are associated with the field f_R whose fluctuations from the background $\delta f_R = f_R(R) - f_R(\bar{R})$ obey a non-linear Poisson equation

$$\nabla^2 \delta f_R = \frac{a^2}{3}\left[\delta R(f_R) - 8\pi G \delta\rho_{\rm m}\right]\,. \tag{3}$$

These field fluctuations act an additional source to the gravitational potential

$$\nabla^2\Psi = 4\pi G a^2 \delta\rho_{\rm m} - \frac{1}{2}\nabla^2\delta f_R\,, \tag{4}$$

whose gradients accelerate non-relativisitic particles as usual. These equations have been solved with N-body techniques for $n = 1$, $n = 2$ and a variety of amplitudes f_{R0} with cosmological parameters $\Omega_{\rm m} = 1 - \Omega_\Lambda = 0.24$, $h = 0.73$ and an initial power spectrum with $A_s = (4.89\times 10^{-5})^2$ at $k = 0.05{\rm Mpc}^{-1}$ and $n_s = 0.958$ [9, 12, 13] [14].

The nonlinearity of Eq. (3) is the key to understanding when the chameleon mechanism does and does not operate. If the field fluctuations are small, they can be linearized as

$$\delta R \approx \left.\frac{dR}{df_R}\right|_{\bar{R}} \delta f_R = 3\lambda_C^{-2}\delta f_R\,, \tag{5}$$

where $\lambda_C = a^{-1}(3df_R/dR)^{1/2}$ is the Compton wavelength of the f_R field in the background. In this case the Poisson equation (4) has the Fourier solution

$$k^2\Psi = -4\pi G\left(\frac{4}{3} - \frac{1}{3}\frac{1}{k^2\lambda_C^2 + 1}\right)a^2\delta\rho_{\rm m}\,, \tag{6}$$

and gravitational forces are enhanced by 1/3 on scales that are below λ_C. We call this the "no-chameleon" limit and for comparison to the chameleon simulations, runs with the same initial conditions using Eq. (6) were conducted. In this limit field fluctuations follow the local gravitational potential on small scales.

As local gravitational potentials of dark matter halos deepen, the field fluctuation can become comparable to the background value f_{R0}. The Compton wavelength can then change significantly from its background value. For the $f(R)$ models described by Eq. (2) the Compton wavelength shrinks so that the force enhancement disappears in deep gravitational potential wells. This ability is called the chameleon mechanism in the literature [4, 5].

Finally, ΛCDM models with the same initial conditions were simulated for comparison. Thus for each simulation box size ($64, 128, 256, 400\ h^{-1}$Mpc) and initial conditions realization (up to 6 each), there are three simulation types: the full $f(R)$ or chameleon, the no-chameleon, and the ΛCDM runs.

To identify dark matter halos in the simulations, we use a spherical overdensity algorithm centered around local density peaks similar to [15]. This method differs slightly from the center of mass of the whole halo approach of [16] used in [13] and is thought to be more directly related to halo observables.

Briefly, to make a crude sorting of density peaks we first assign particles to the grid using the cloud-in-cell (CIC) scheme. Starting at the highest density grid point, we grow a halo until the enclosed spherical overdensity reaches $\Delta = \rho_m/\bar{\rho}_m = 200$ defining a radius r_{200}. We then refine the center of the halo by solving for the center of mass iteratively in shrinking radii from $r_{200}/3$ to $r_{200}/15$ or until only 20 particles are found within the smoothing radius. We then regrow the halo around this center until the spherical overdensity criteria is met. The halo mass M_{200} is the sum of mass of all particles enclosed within this halo radius r_{200}. Due to lack of spatial resolution we only count halos with more than $N_{\rm min} = 800$ particles.

Compared with the halo center of mass approach, this algorithm tends to break up regions with large subclumps into separate halos reducing the number of high mass halos by up to 10%. Its effect on the relative abundance between the $f(R)$ simulations and the ΛCDM simulations is much smaller since it affects the two in the same way.

We construct the mass function of dark matter halos for the various simulations by adding up the number of halos within a certain mass bin from different boxes directly, which implicitly weights the simulations by volume. To estimate the errors on the mass function enhancements over ΛCDM, we bootstrap resample the differences, with replacement within each of the different box sizes.

III. CHAMELEON MASS FUNCTION

The mass function or differential abundance of dark matter halos for the various $f(R)$ models and simulations have previously been studied in [9, 13]. In the large field regime of $|f_{R0}| > 10^{-5}$, the excess abundance appears mainly in the rarest halos and these results are well-modeled by simple modifications to spherical collapse predictions. In the small field regime $|f_{R0}| < 10^{-5}$ which is comparable to or smaller than the depth of the gravitational potential wells of cluster mass sized halos, the chameleon mechanism shuts off the excess in the abundance of these halos.

Instead, in this regime, the chameleon simulations produce an abundance of intermediate sized halos that is in

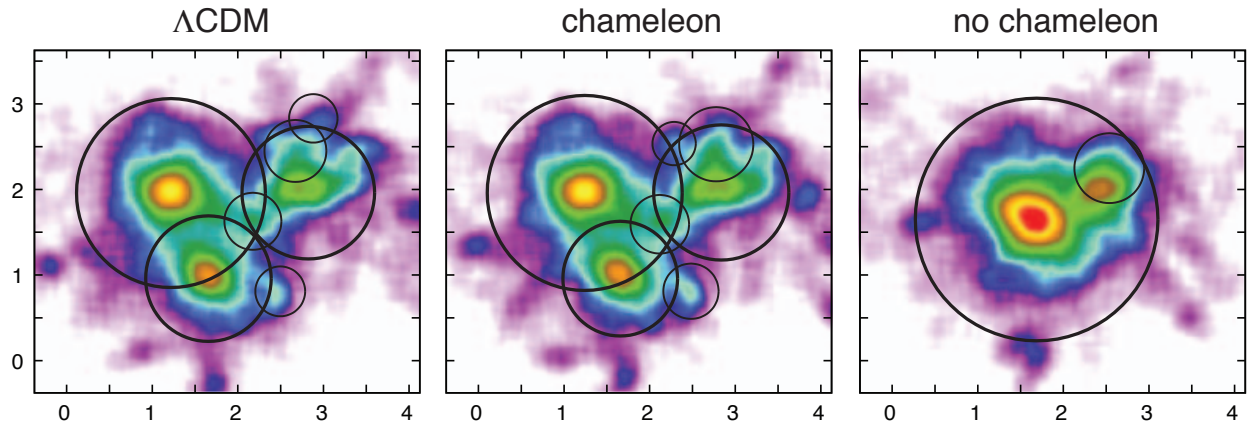

FIG. 1. Projected 2D density maps and identified halos for the 3 types of simulations: ΛCDM, $f(R)$ chameleon, and no-chameleon models ($|f_{R0}| = 10^{-6}, n = 1$). Axes are in h^{-1}Mpc and the color map represents the logarithmic density on a $0.25h^{-1}$Mpc grid projected across a $4.25h^{-1}$Mpc depth. Halos are denoted with circles (thick lines: > 800 particles; thin lines $100 - 800$ particles plotted for reference). The largest halos in each case from left to right are 7.5×10^{13}, 8.2×10^{13} and $1.6 \times 10^{14} h^{-1} M_\odot$ respectively showing that between ΛCDM and the chameleon case halos mainly grow in mass whereas between the chameleon and no-chameleon case a major merger has occurred.

excess of both the no-chameleon simulations and the predictions with the full 1/3 enhancement of forces everywhere [13].

To understand this result, we can compare the full and no-chameleon simulations in the $n = 1$, $|f_{R0}| = 10^{-6}$ model where the chameleon effect is the strongest. Since the ΛCDM, chameleon and no-chameleon models are simulated with the same initial condition realization, we can examine regions in the simulations associated with intermediate mass halos. In Fig. 1 we show an example. The halos in the chameleon run are very similar to those in the ΛCDM run only slightly more massive. On the other hand, in the no-chameleon run several of the intermediate sized halos have merged into one high mass halo.

Correspondingly, the no-chameleon simulations show an excess in the abundance of high mass halos which compensate the excess of intermediate mass halos in the full runs (see Fig. 2). Those halos that under the no-chameleon assumption would have merged to form high mass halos no longer do in the chameleon simulations causing a pile up effect at intermediate masses.

The results are consistent with mass conservation in the intermediate to high mass halo regime. To characterize this merging effect, we model the mass function based on the Press-Schechter ansatz that all of the mass in the universe is in halos of some mass. We automatically conserve mass in halos if we only vary the ingredients of the models.

The standard prescription based on the linear power spectrum requires modification however. In this prescription large masses are related to large scales through

$$\sigma^2(M(R)) = \int \frac{d^3k}{(2\pi)^3} |W(kR)|^2 P_L(k)\,, \qquad (7)$$

the variance of the linear density field convolved with a tophat of radius R, with Fourier transform $W(kR)$, that encloses the mass M at the background density. On the other hand, the chameleon mechanism operates on large masses and *small* scales. Our approach is to retain a mass function construction based on a $\sigma(M)$ but generalize its relationship to the linear power spectrum in Eq. (7) such that it no longer represents the rms of the linear density field of the $f(R)$ model. We follow the pa-

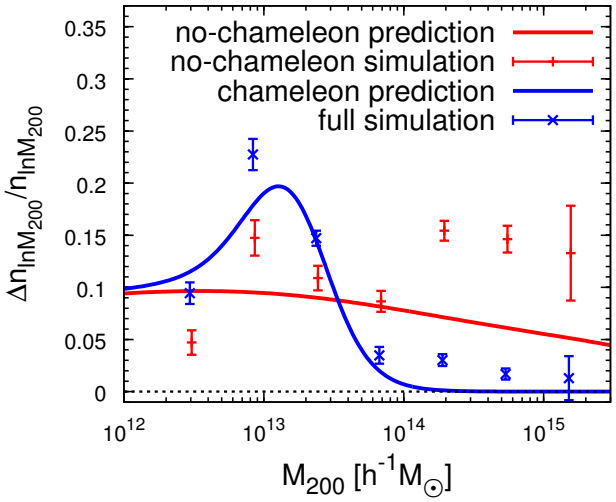

FIG. 2. Simulation results and parametrized post-Friedmann (PPF) fit for the mass function excess of $f(R)$ with $n = 1$, $|f_{R0}| = 10^{-6}$ over ΛCDM. Chameleon simulations show not only a suppression of the high mass enhancement compared with no-chameleon runs but also a larger excess at intermediate masses, here $\sim 10^{13} h^{-1} M_\odot$. These features can be fit by an interpolation between the limiting $\sigma(M)$ cases across a threshold mass $M_{\rm th} = 1.345 \times 10^{13} h^{-1} M_\odot$ with $\alpha = 2.448$ for the rapidity of the transition (see Eq. 10).

rameterized post-Friedmann (PPF) approach of taking this generalization to be an interpolation between modified and unmodified gravity [10].

We take the mass function to be universal in the virial mass $M_{\rm v}$

$$n_{\ln M_{\rm v}} \equiv \frac{dn}{d\ln M_{\rm v}} = \frac{\bar\rho_m}{M_{\rm v}}\frac{d\ln\nu}{d\ln M_{\rm v}}\nu f(\nu)\,, \qquad (8)$$

where $\nu = \delta_c/\sigma(M_{\rm v})$ and $\int f(\nu)d\nu = 1$. For the Sheth-Torman mass function [17]

$$\nu f(\nu) = A\sqrt{\frac{2}{\pi}a\nu^2}[1+(a\nu^2)^{-p}]\exp(-a\nu^2/2)\,, \qquad (9)$$

with $a = 0.75$, $p = 0.3$ and A given by $\int d\nu f(\nu) = 1$ as $A = 0.3222$. We adopt $\Delta_{\rm v} = 390$ and $\delta_c = 1.673$ which are the values that match the ΛCDM predictions for $\Omega_m = 0.24$. Previous attempts to model the simulation results were based on adjusting $\Delta_{\rm v}$ and δ_c in a spherical collapse motivated range using $\sigma(M)$ from the linear power spectrum of the $f(R)$ model. That technique captures the high mass end $M > 10^{14}h^{-1}M_\odot$ for both large and small fields but failed in the $M < 10^{14}h^{-1}M_\odot$ in the small field regime.

Here we instead leave $\Delta_{\rm v}$ and δ_c fixed but interpolate between limiting behaviors of $\sigma(M)$. For high masses $\sigma(M)$ should approach the ΛCDM result $\sigma_{\Lambda{\rm CDM}}(M)$ due to the chameleon mechanism. For small masses, it should approach the prediction of $f(R)$ linear theory with enhanced forces $\sigma_{f_R}(M)$. We thus take a chameleon PPF transition between these fixed limits

$$\sigma(M) = \frac{\sigma_{f_R}(M) + (M/M_{\rm th})^\alpha\sigma_{\Lambda{\rm CDM}}(M)}{1+(M/M_{\rm th})^\alpha}\,. \qquad (10)$$

In Fig. 3, we show an example for the $|f_{R0}| = 10^{-6}$, $n = 1$ model. By definition, the fraction of the universe tied up in halos above an $M \ll M_{\rm th}$ is conserved independently of the transition

$$\begin{aligned} F(>M) &= \int_M^\infty \frac{dn}{d\ln M_{\rm v}}\frac{M_{\rm v}}{\bar\rho_m}d\ln M_{\rm v} \\ &= \int_{\delta_c/\sigma(M)}^\infty d\nu f(\nu) \\ &\approx \int_{\delta_c/\sigma_{f_R}(M)}^\infty d\nu f(\nu), \quad M \ll M_{\rm th}\,. \end{aligned} \qquad (11)$$

Given this $(M_{\rm th},\alpha)$ parameterization, we fit the simulation results of the $|f_{R0}| = 10^{-6}$, $n = 1$ model. We first convert the parameterized mass function defined at the virial overdensity to M_{200} assuming an Navarro-Frenk-White profile [18]. We then integrate the resulting $n_{\ln M_{200}}$ over a tophat in $\ln M_{200}$ of the bin size which effectively smooths the predictions to our simulation binning. Finally, using the bootstrap errors we minimize the χ^2 between the model and the simulation data and determine that $M_{\rm th} = 1.345\times10^{13}h^{-1}M_\odot$ and $\alpha = 2.448$ yield the best fit (see Fig. 2).

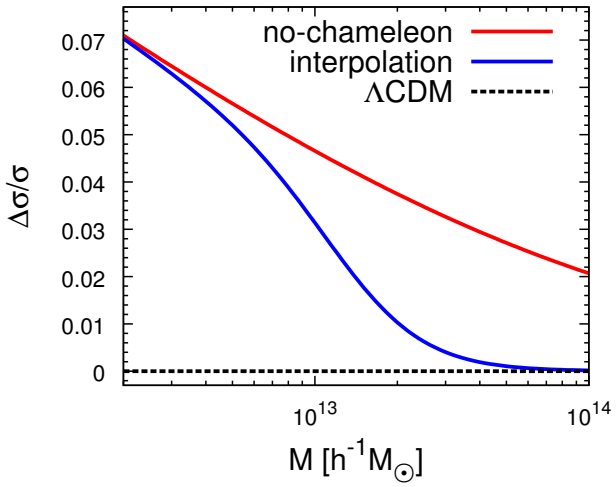

FIG. 3. Fractional change in $\sigma(M)$ between the linear $f(R)$ prediction (red, upper curve, $|f_{R0}| = 10^{-6}$, $n = 1$) and the linear ΛCDM prediction (black, dashed curve). The PPF prescription interpolates between these two limits (blue, middle curve) with the transition parameters $M_{\rm th} = 1.345\times10^{13}h^{-1}M_\odot$ and $\alpha = 2.448$.

This single choice of parameters $(M_{\rm th},\alpha)$ can be scaled to fit all of the simulations without introducing any additional degrees of freedom. Given that the critical mass for the chameleon scales with the background field value as $|f_{R0}|^{3/2}$ [9], we take

$$M_{\rm th} = 1.345\times10^{13}\left(\frac{|f_{R0}|}{10^{-6}}\right)^{3/2}h^{-1}M_\odot\,. \qquad (12)$$

In Fig. 4 we compare the results of the various $(|f_{R0}|, n)$ simulations to this universal scaling.

IV. CHAMELEON POWER SPECTRUM

The chameleon mass function is the starting point for halo modeling of cosmological observables. For example, under the halo model, the dark matter power spectrum is described by density correlations within halos and between halos integrated over the mass function. For the same wavenumber k, the chameleon mechanism affects density correlations associated with some but not all dark matter halos.

Under the halo model, the power spectrum in the deeply nonlinear regime is determined by density correlations within single halos. The power spectrum in this regime can be modeled with the 1 halo term

$$P_H(k) = \int d\ln M_{\rm v} n_{\ln M_{\rm v}}\left(\frac{M_{\rm v}}{\rho_m}\right)^2|y(k,M_{\rm v})|^2\,, \qquad (13)$$

where $y(k,M)$ is the Fourier transform of the density profile truncated at $r_{\rm v}$. For both ΛCDM and $f(R)$ the halo profiles are well characterized by the NFW form [13].

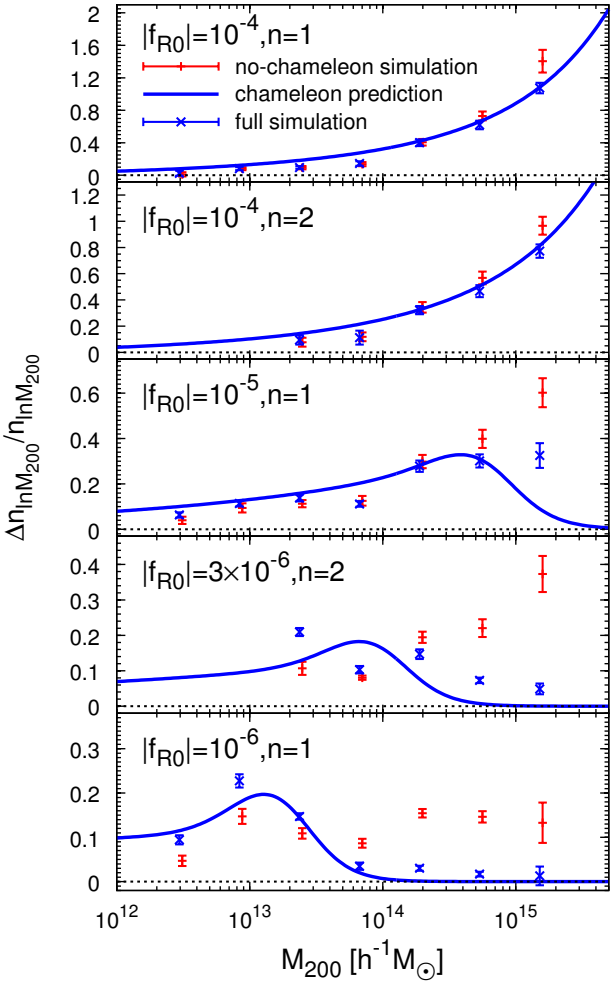

FIG. 4. Chameleon mass function excess for different $f(R)$ models. A universal fit to $\sigma(M)$ with $\alpha = 2.448$ and $M_{\rm th} = 1.345\times10^{13}(|f_{R0}|/10^{-6})^{3/2}h^{-1}M_\odot$ fits the range of $(|f_{R0}|, n)$ simulations comparably well.

We take a concentration given by [19]

$$c = 9(M_{\rm v}/M_*)^{-0.13}\,, \tag{14}$$

where M_* is defined via $\sigma(M_*) = \delta_c$. Thus the main difference in this regime for the power spectra of the models should come from the difference between the mass functions.

As noted in [13], without a description of the chameleon mass function, the one halo contributions for $|f_{R0}| < 10^{-5}$ are overestimated on intermediate scales where contributions from groups and clusters dominate. While this effect can be modeled with fitting parameters that depend explicitly on the field value $|f_{R0}|$ [20], the halo model provides a universal description of the chameleon effect on the power spectrum. In addition it provides better physical insight into its origin and relation to other observables such as the mass function and higher point functions. In Fig. 5, we show the PPF predictions based on the mass function enhancement for the 1 halo term compared with the no-chameleon mass function predictions for $|f_{R0}| = 10^{-6}$, $n = 1$. The chameleon effect suppresses 1 halo power on scales less than a few h/Mpc.

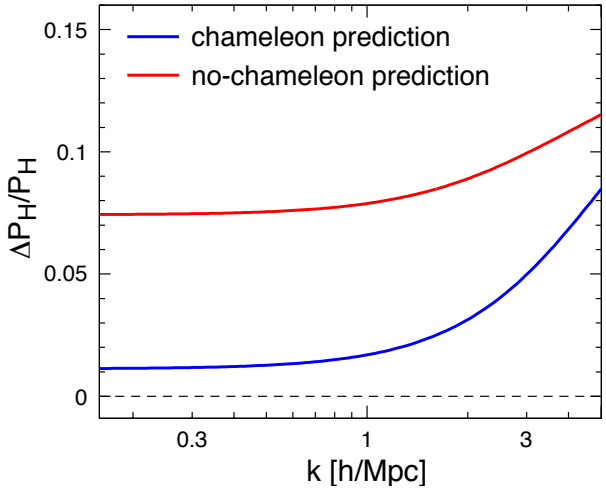

FIG. 5. 1 halo power spectrum enhancement of $f(R)$ over ΛCDM. PPF predictions are shown for the $|f_{R0}| = 10^{-6}$, $n = 1$ model with and without the chameleon modeling of the mass function effects. Without the chameleon modeling, high mass halos contribute excess power in the quasilinear regime of $k \lesssim$ few h/Mpc not found in the simulations.

For a full model of the power spectrum, we must include the large scale linear regime. In the linear regime, the halo model describes the power spectrum in terms of the correlation between two different halos. Using a mass function construction that places all of the mass in halos and the halo bias of the peak-background split guarantees that the two halo term simply returns the input linear power spectrum. Unfortunately, in order to describe the power spectrum at intermediate k between the linear and nonlinear regimes, the halo model requires complications such as halo exclusion to maintain accuracy (e.g. [21–23]).

We instead take the phenomenological approach of Halofit [24] and seek an interpolation between the known linear behavior and the 1 halo model for the deeply nonlinear behavior spectrum. Specifically we take

$$\frac{k^3P(k)}{2\pi^2} = \Delta^2(k) = \Delta^2_Q(k) + \Delta^2_H(k)\,. \tag{15}$$

Here $\Delta^2_H(k)$ is the dimensionless power spectrum derived from $P_H(k)$ and $\Delta^2_Q(k)$ is related to the linear theory power spectrum $\Delta^2_L(k)$ by

$$\Delta^2_Q(k) = \Delta^2_L\frac{[1+\Delta^2_L(k)]^{\beta_n}}{1+\alpha_n\Delta^2_L(k)}\exp(-y/4-y^2/8)\,, \tag{16}$$

where $y = k/k_\sigma$ determines the scale of the transition to the 1 halo term and α_n, β_n are fitting parameters to adjust the shape of the transition.

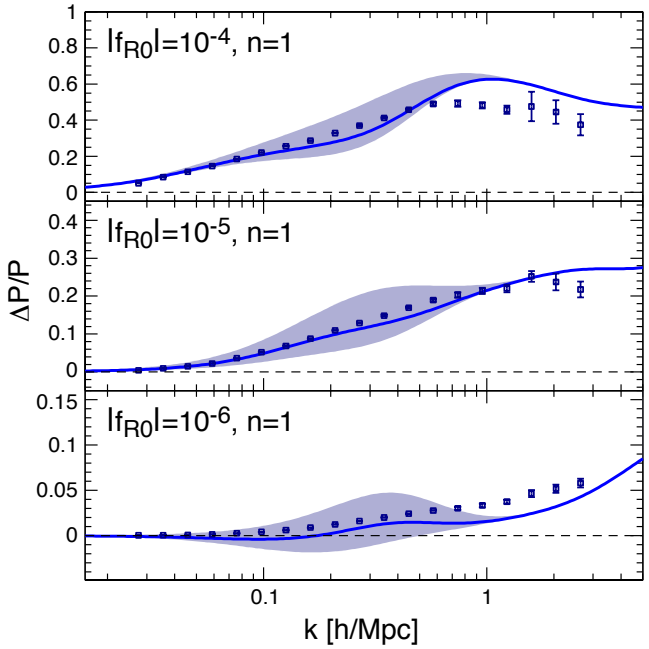

FIG. 6. Power spectrum enhancement for $n = 1$ models compared with PPF predictions. Blue bands represent a range of Halofit parameters α_n, β_n where the upper limit comes from the linear ΛCDM power spectrum and the lower from the linear $f(R)$ power spectra. Solid blue lines represent the average of the two extreme values of the parameters and is a good prescription for all cases.

Halofit describes the transition scale in terms of the Gaussian filtered variance

$$\sigma_G^2(R) = \int d\ln k\, \Delta_{\rm L}^2 e^{-k^2R^2} \tag{17}$$

as $\sigma_G(k_\sigma^{-1}) = 1$. Rather than refit the transition parameters α_n, β_n, we examine the limiting cases predicted by Halofit from the linear power spectra of ΛCDM and $f(R)$. The Halofit prescription is to take the local slope

$$n_{\rm eff} \equiv -3 - \frac{d\ln\sigma_G^2(R)}{d\ln R}\Big|_{\sigma_G=1}, \tag{18}$$

and characterize

$$\begin{aligned}\alpha_n &= 1.3884 + 0.3700 n_{\rm eff} - 0.1452 n_{\rm eff}^2,\\ \beta_n &= 0.8291 + 0.9854 n_{\rm eff} + 0.3401 n_{\rm eff}^2.\end{aligned} \tag{19}$$

In Fig. 6 we show the simulation results compared with the PPF predictions with a range of α_n and β_n given by linear ΛCDM for the upper limit and linear $f(R)$ for the lower. Simulation results lie mainly in between these two limits and in fact a simple average of the two α_n and β_n values provides a good description for all models.

V. DISCUSSION

In the $f(R)$ model, the chameleon mechanism mediates a restoration of general relativity and ordinary Newtonian forces in deep gravitational potential wells. We have shown that the main impact of the chameleon mechanism on cosmological statistics that depend on the dark matter halo distribution can be simply described by a universal scaling for the transition between modified and unmodified forces in mass or gravitational potential. This type of transition should be contrasted with phenomenological approaches that implement the transition as a function of physical scale (e.g. [25]) or with models that implement the Vainshtein mechanism where the transition is a function of density [10].

In the mass function, the chameleon mechanism leads to a doubly enhanced abundance near the transition. In the simulations, this enhancement is associated with smaller mass halos still growing to the transition mass due to enhanced forces but transition mass halos no longer merging into high mass halos due to the restoration of ordinary forces. In our description, this mass conservation property is enforced through the Press-Schechter assumption that all of the dark matter is in halos of some mass. With this assumption, we can fit the mass function results across a wide range in $f(R)$ models with two constants: the scaling of the transition mass to the background field and the rapidity of the transition in mass.

With a calibration of the mass function and the simulation result that halo profiles as a function of mass are largely unchanged, we can construct predictions for the N-point functions. In particular for the power spectrum, including the chameleon effects on the mass function bring predictions for the power spectrum excess down in agreement with the simulations. We have provided a simple modification to the Halofit prescription to bridge the linear and nonlinear regimes. For the higher N-point functions, the model predicts that the results in the deeply nonlinear regime should scale mainly with the single degree of freedom of the mass function.

Moreover, by describing these effects as enhancements over the ΛCDM mass function and power spectrum with a physically well-motivated extrapolation to low masses and small scales rather than an absolute prediction of $f(R)$ statistics, one can use state-of-the-art simulations and calibrations for ΛCDM predictions and look for a parameterized excess over those in the data (see, e.g. [7]). These techniques should enable tests of the $f(R)$ model with weak lensing and other statistics that require large dynamic range and precision.

Acknowledgments: We thank Simone Ferraro and Fabian Schmidt for useful discussions. YL and WH were supported by the Kavli Institute for Cosmological Physics (KICP) at the University of Chicago through grants NSF PHY-0114422 and NSF PHY-0551142 and an endowment from the Kavli Foundation and its founder Fred Kavli. WH was additionally supported by U.S. Dept. of En-

ergy contract DE-FG02-90ER-40560 and the David and Lucile Packard Foundation. Computational resources for the cosmological simulations were provided by the KICP-Fermilab computer cluster.

[1] S. Capozziello, Int.J.Mod.Phys., **D11**, 483 (2002), arXiv:gr-qc/0201033 [gr-qc].
[2] S. Nojiri and S. D. Odintsov, Phys. Rev., **D68**, 123512 (2003), hep-th/0307288.
[3] S. M. Carroll, V. Duvvuri, M. Trodden, and M. S. Turner, Phys. Rev., **D70**, 043528 (2004), astro-ph/0306438.
[4] D. F. Mota and J. D. Barrow, Phys. Lett., **B581**, 141 (2004), arXiv:astro-ph/0306047.
[5] J. Khoury and A. Weltman, Phys. Rev. D, **69**, 044026 (2004), arXiv:astro-ph/0309411.
[6] W. Hu and I. Sawicki, Phys. Rev. D, **76**, 064004 (2007), arXiv:0705.1158.
[7] F. Schmidt, A. Vikhlinin, and W. Hu, Phys. Rev., **D80**, 083505 (2009), arXiv:0908.2457 [astro-ph.CO].
[8] L. Lombriser, A. Slosar, U. Seljak, and W. Hu, (2010), arXiv:1003.3009 [astro-ph.CO].
[9] S. Ferraro, F. Schmidt, and W. Hu, Phys.Rev., **D83**, 063503 (2011), arXiv:1011.0992 [astro-ph.CO].
[10] W. Hu and I. Sawicki, Phys. Rev. D, **76**, 104043 (2007), arXiv:0708.1190.
[11] K. Koyama, A. Taruya, and T. Hiramatsu, Phys. Rev., **D79**, 123512 (2009), arXiv:0902.0618 [astro-ph.CO].
[12] H. Oyaizu, M. Lima, and W. Hu, Phys. Rev., **D78**, 123524 (2008), arXiv:0807.2462 [astro-ph].
[13] F. Schmidt, M. V. Lima, H. Oyaizu, and W. Hu, Phys. Rev., **D79**, 083518 (2009), arXiv:0812.0545 [astro-ph].
[14] This corrects a 3% absolute error in the initial conditions reported in [12] but does not change results relative to ΛCDM significantly.
[15] J. L. Tinker *et al.*, Astrophys. J., **688**, 709 (2008), arXiv:0803.2706 [astro-ph].
[16] C. Lacey and S. Cole, Mon. Not. R. Astron. Soc., **271**, 676 (1994), arXiv:astro-ph/9402069.
[17] R. Sheth and B. Tormen, Mon. Not. R. Astron. Soc., **308**, 119 (1999).
[18] W. Hu and A. V. Kravtsov, Astrophys. J., **584**, 702 (2003), arXiv:astro-ph/0203169.
[19] J. S. Bullock, T. S. Kolatt, Y. Sigad, R. S. Somerville, A. V. Kravtsov, A. A. Klypin, J. R. Primack, and A. Dekel, Mon. Not. R. Astron. Soc., **321**, 559 (2001), arXiv:astro-ph/9908159.
[20] G.-B. Zhao, B. Li, and K. Koyama, Phys.Rev., **D83**, 044007 (2011), arXiv:1011.1257 [astro-ph.CO].
[21] M. Magliocchetti and C. Porciani, Mon.Not.Roy.Astron.Soc., **346**, 186 (2003), arXiv:astro-ph/0304003 [astro-ph].
[22] J. L. Tinker, D. H. Weinberg, Z. Zheng, and I. Zehavi, Astrophys.J., **631**, 41 (2005), arXiv:astro-ph/0411777 [astro-ph].
[23] M. Cacciato, F. C. d. Bosch, S. More, R. Li, H. Mo, *et al.*, Mon.Not.Roy.Astron.Soc., **394**, 929 (2009), arXiv:0807.4932 [astro-ph].
[24] R. E. Smith, J. A. Peacock, A. Jenkins, S. D. M. White, C. S. Frenk, F. R. Pearce, P. A. Thomas, G. Efstathiou, and H. M. P. Couchman, Mon. Not. R. Astron. Soc., **341**, 1311 (2003), arXiv:astro-ph/0207664.
[25] L. Amendola, M. Kunz, and D. Sapone, JCAP, **0804**, 013 (2008), arXiv:0704.2421 [astro-ph].